

## Quasi-Differential Neutron Scattering Measurements of $^{238}\text{U}$

A.M. Daskalakis, R.M. Bahrn, E.J. Blain, B.J. McDermott, S. Piela, and Y. Danon  
*Gaertner LINAC Center, Rensselaer Polytechnic Institute, Troy, New York 12180 email:daskaa@rpi.edu*

D.P. Barry, G. Leinweber, R.C. Block, and M.J. Rapp  
*Bechtel Corp., Knolls Atomic Power Laboratory, P.O. Box 1072, Schenectady, New York 12301*

### INTRODUCTION

Uranium-238 is used extensively in nuclear reactor cores. Its nuclear properties have a significant effect on many aspects of the entire fuel cycle process from enrichment facilities and power production to nuclear waste storage facilities. In order to safely design such systems, an accurate evaluation of neutron interactions with  $^{238}\text{U}$  is required. This paper describes a process of quantifying differences between evaluations through the energy-angle distribution of neutrons from scattering and fission of  $^{238}\text{U}$  using the Rensselaer Polytechnic Institute (RPI) neutron scattering system.

Differential neutron scattering data are available in evaluated nuclear data libraries such as ENDF/B-VI.8 and VII.0 [1], JEFF-3.1 [2], and JENDL-4.0 [3] which often contain discrepancies. In order to compare the different evaluations, a benchmarking process was performed comparing experimental data to models. With this experiment, there are several factors that differentiate it from a typical double differential neutron scattering experiment [4]. The main factor was the use of a white neutron source that was incident onto the sample. In addition, multiple scattered elastic and inelastic interactions along with fission neutrons are produced by the  $^{238}\text{U}$  sample and recorded by the detectors. This increased the signal-to-background ratio, which reduced the statistical errors and accentuated library differences due to multiple interactions. This led to the terminology describing the experiment as quasi-differential neutron scattering [5].

### EXPERIMENTAL DESCRIPTION

#### Experimental Setup

The RPI Electron Linear Accelerator (LINAC) generates a pulse of neutrons using high-energy electrons. The electrons are accelerated to an energy of  $\sim 60$  MeV and collide with a tantalum neutron-producing target [6]. Within the target, electrons create bremsstrahlung radiation that interacts with the tantalum plates creating neutrons through the photo-nuclear process. The neutrons travel along an evacuated flight path to a distance of  $\sim 30$  meters where the RPI scattering system is located. The time-of-flight (TOF) method was used to determine the incident neutron's energy. A 1.9 cm filter of depleted

uranium was placed in the beam to reduce the gamma flash radiation produced by the target. The neutron beam was collimated to a diameter of 7.62 cm incident on the scattering sample.

Each detector's gain was matched at the Compton edge of 0.511 MeV annihilation gammas from a  $^{22}\text{Na}$  source by adjusting the photomultiplier voltage. Gain alignment was checked several times throughout the experiment to identify and minimize detector drifts. During the scattering experiment, the array of eight detectors was arranged at various scattering angles around a sample. A graphite reference sample and  $^{238}\text{U}$  were cycled into the neutron beam using a programmable sample changer. The LINAC was operated with a repetition rate of 400 pulses per second with a 6 nanosecond electron burst width. The average current on the target was  $\sim 8 \mu\text{A}$ .

Eight ELJEN Technologies EJ301 liquid scintillator proton recoil fast neutron detectors were used for the experiments and were located at different angles relative to the incident neutron beam. Each measures 12.7 cm in diameter by 7.62 cm in length and is coupled to a 12.7 cm diameter Photonis XP4572/B photomultiplier tube (PMT). A CAEN unit, model 1733N, supplies negative high voltage to each of the detectors. The raw signals from the detectors were fed into an Agilent-Acqiris AP240 digitizer which converted the analog pulse into an 8-bit digital signal, an onboard field-programmable gate array (FPGA) transfers the data only if a pulse exceeds the predefined threshold. Each converted signal consists of 120 channels that contain the first 120 nanoseconds of pulse data. This interval of time was selected based on the EJ301 liquid scintillator response time. A maximum of 128,000 detector pulses per second can be handled by the system, restricted by the data transfer rate [7].

Fluctuations in the beam intensity were recorded by two moderated fission chambers located  $\sim 9$  meters from the target. The monitor data were also used to adjust background and normalize it to the  $^{238}\text{U}$  data and graphite data.

#### Flux and Detector Efficiency Measurement

The RPI neutron scattering system has been used to compare neutron data libraries with measurements of zirconium [5], beryllium [7], and molybdenum [7]. In these publications the detector efficiency and flux were determined by using  $^6\text{Li}$  glass measurements and

SCINFUL [8] modeling of proton-recoil liquid scintillators detectors [7]. To improve the accuracy of the scattering system, new measurements were performed to obtain independent detector efficiencies for each neutron scattering detector.

To acquire the efficiency, the response of each detector (EJ301 liquid-scintillator) to the neutron flux was obtained. The position of the detector for the in-beam experiment was in the center of the neutron beam where one detector records data at a time. The counts,  $C$ , based on the incident flux,  $\phi$ , and the detector's intrinsic efficiency,  $\eta$ , at a given time of flight,  $t$ , were recorded.

$$C(t) = \phi(t) \cdot \eta(t) \quad (1)$$

The flux in Eq. (1) was determined by an independent measurement conducted with a  $^{235}\text{U}$  fission chamber. The fission chamber was placed in the same position as the detector so it received the same incident flux. Since the fission cross section for  $^{235}\text{U}$  is well known it was used to develop the energy dependent neutron source term for an MCNP model [9]. All experimental data from in-beam detectors were dead-time corrected.

In the MCNP model an F2 tally with intrinsic efficiency of unity was used to record the neutron response at the detector position. The results were integrated over a region of interest (ROI), 0.5 to 20 MeV, in order to normalize the MCNP flux calculation to experimental in-beam data. The relative efficiency of each detector with respect to each other was determined by dividing the experimental data by the normalized MCNP flux calculation. This process was validated by additional simulations that included the detector's relative efficiency. The calculated results were compared with the experimental in-beam data.

### Data Collection and Analysis

Open beam (no sample) data associated with the graphite and  $^{238}\text{U}$  sample were collected periodically throughout the experiment and used as a measure of the background count rate. All data collected by the EJ301 detectors was processed using pulse shape analysis (PSA) to discriminate neutrons from photons. The ROOT data analysis framework was used for this analysis [10]. Detailed descriptions of the PSA and post processing can be found in previous work [7]. After PSA the background subtracted data,  $D$ , was determined by subtracting the monitor normalized open data from the sample data.

$$D = D_S - \frac{M_S}{M_O} \cdot D_O \quad (2)$$

$M_S$  and  $M_O$  are the beam monitor counts for the sample and open, respectively.  $D_S$  and  $D_O$  represent the counts

collected for the sample and open, respectively. The standard error propagation formula with respect to Eq. (2) was applied, yielding the statistical error in the counts per channel [11].

A method was developed to compare the MCNP calculations to experimental data. The results of the normalized MCNP calculation,  $C$ , were summed and divided by the sum of the experiment data,  $E$ , for each TOF channel,  $i$ , in a ROI. This was defined as the  $(C/E)_{ROI}$  value for a given energy region at a certain scattering angle.

$$\left(\frac{C}{E}\right)_{ROI} = \frac{\sum_{i=E_{\min}}^{E_{\max}} C_i}{\sum_{i=E_{\min}}^{E_{\max}} E_i} \quad (3)$$

The channels for a particular ROI span from  $E_{\min}$  through  $E_{\max}$ . The MCNP calculations were normalized to match the graphite reference sample. This is discussed further in the next section. More detailed information regarding  $C/E$  can be found in Reference [5].

### Quasi-Differential Scattering Measurements

The TOF, and therefore the neutron interaction energy, was determined by the time required by the neutrons to traverse the distance between the neutron target and sample,  $L_1$ , plus distance from the sample to the detector,  $L_2$ . The total TOF,  $t$ , for incident neutrons with energy,  $E_1$ , can be expressed as:

$$t = \left(\frac{L_1}{c}\right) \cdot \frac{1}{\sqrt{1 - \left(\frac{m_n c^2}{E_1 + m_n c^2}\right)^2}} + \left(\frac{L_2}{c}\right) \cdot \frac{1}{\sqrt{1 - \left(\frac{m_n c^2}{E_2 + m_n c^2}\right)^2}} \quad (4)$$

where  $m_n$  is the rest mass of the neutron and  $c$  is the speed of light in a vacuum. In the experiment the distance  $L_1 = 30.07$  m and  $L_2 = 0.50$  m. Following a scattering collision the energy of the neutron was reduced to  $E_2$ . In such a case due to the small energy loss per collision,  $E_1 \approx E_2$ , and thus,  $t_2 \ll t_1$  so that the effective flight distance is defined as  $L = L_1 + L_2$ . For fission neutrons  $E_1$  can be higher or lower than  $E_2$ ; however, because  $L_1 \gg L_2$  both  $L = L_1 + L_2$  and  $t = t_1 + t_2$  were used to obtain the effective incident neutron energy at TOF,  $t$ .

$$E(t) \approx m_n c^2 \cdot \left( \frac{1}{\sqrt{1 - \left(\frac{L}{c \cdot t}\right)^2}} - 1 \right) \quad (5)$$

A cylindrical high purity graphite sample 7.5 cm in diameter by 7 cm thick was used as a reference sample [7]. MCNP calculations modeled the neutron interaction with graphite for all detectors. In order to compare the MCNP calculation with the experimental model, normalization was applied to the calculations. The normalization was obtained by dividing the integrated graphite experimental data by the integrated MCNP calculation. Each was integrated from 0.5 to 20 MeV to find a normalization ratio unique to each detector. The values were averaged to form a normalization factor, which was applied to the MCNP calculation. The standard deviation of the distribution of individual normalization factors for each detector was included as part of the systematic error on the measurement. In addition, because graphite was used as a reference, the deviation in its  $(C/E)$  from unity could be interpreted as a systematic error in the  $(C/E)$  of  $^{238}\text{U}$ .

A depleted uranium (0.2 at%  $^{235}\text{U}$ ) cylindrical sample 3.8 cm in diameter by 0.98 cm thick was used in the experiment and modeled in MCNP. The normalized MCNP calculations were then compared with experimental data to determine which datasets are best to use in various energy regions and scattering angles.

## RESULTS

Graphite results for the detector at  $60^\circ$  relative to the incident beam are shown in Fig. 1 together with the MCNP simulation. The graphite  $(C/E)$  for the entire energy region, 0.5 to 20 MeV, was 0.985; therefore, 1.5% can be considered a systematic error in graphite and  $^{238}\text{U}$ .

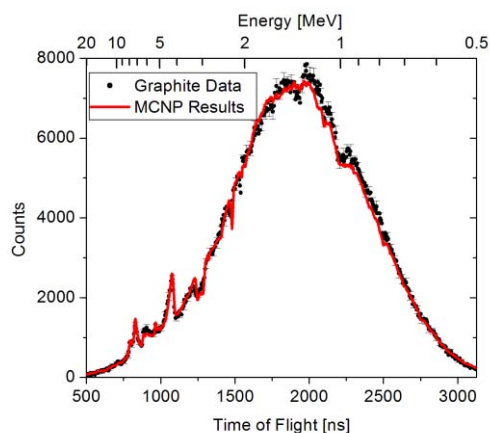


Fig. 1. Experimental data at 60 degrees compared with the MCNP calculation of neutron interactions with the graphite sample.

The systematic error on the normalization value was  $\sim 0.7\%$  and was considered constant throughout all energy regions. The statistical error associated with graphite was small with respect to the deviation from unity in  $(C/E)$ . Fig. 2 shows the different datasets compared with the experimental data for  $^{238}\text{U}$ .

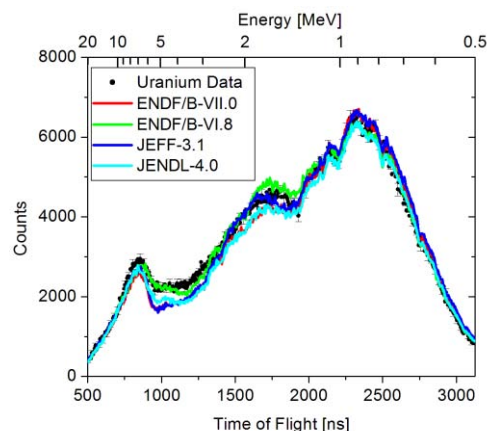


Fig. 2. Experimental data at 60 degrees compared with several libraries using MCNP calculations of neutron interactions with the  $^{238}\text{U}$  sample.

Comparisons of calculations to experimental data were made over the entire energy region, 0.5 to 20 MeV, and smaller energy ROIs. Table I shows how each of the datasets behaves over the entire energy region, 0.5 to 20 MeV. An estimate of the total error for the  $^{238}\text{U}$   $(C/E)$  value in the entire energy region or in smaller ROIs can be considered to be the combination of the statistical error, the normalization error, and the deviation from unity for the graphite  $(C/E)$  value in a given ROI. Deviations from unity greater than the sum of the errors indicate the library does not reproduce the experimental data using the MCNP model.

Table I.  $(C/E)$  at 60 degrees for  $^{238}\text{U}$  over the entire energy range. The systematic error on the normalization is 0.007 (0.7%) and  $(C/E)$  for graphite is 0.015 (1.5%).

Dataset	C / E in the ROI
ENDF/B-VII.0	$0.970 \pm 0.001$
ENDF/B-VI.8	$1.005 \pm 0.001$
JEFF-3.1	$0.997 \pm 0.001$
JENDL-4.0	$0.947 \pm 0.001$

Over the entire energy region there are distinguishable differences between the  $(C/E)$  for  $^{238}\text{U}$  using ENDF/B-VII.0 and JENDL-4.0 datasets compared to experimental data. ENDF/B-VI.8 and JEFF-3.1 datasets reproduce the experiment within the precision of the measurement. However, significant differences between MCNP calculations and experimental data were also observed for smaller ROIs. The errors associated

with the smaller ROIs represent how well the  $^{238}\text{U}$  data in that particular region matches the MCNP calculation. The statistical error and graphite ( $C/E$ ) deviation from unity differ in each energy region. The  $^{238}\text{U}$  ( $C/E$ ) values for smaller ROI and associated errors are shown in Table II.

Table II. ( $C/E$ ) at 60 degrees for  $^{238}\text{U}$  over smaller energy ranges. The systematic error on the normalization is 0.007 (0.7%).

ROI 1 – 10 to 20 MeV with ( $C/E$ ) for graphite of 0.051 (5.1%)	
ENDF/B-VII.0	$0.969 \pm 0.010$
ENDF/B-VI.8	$0.989 \pm 0.010$
JEFF-3.1	$1.007 \pm 0.010$
JENDL-4.0	$0.972 \pm 0.010$
ROI 2– 5 to 10 MeV with ( $C/E$ ) for graphite of 0.001 (0.1%)	
ENDF/B-VII.0	$0.852 \pm 0.004$
ENDF/B-VI.8	$0.965 \pm 0.004$
JEFF-3.1	$0.882 \pm 0.004$
JENDL-4.0	$0.904 \pm 0.004$
ROI 3 – 2 to 5 MeV with ( $C/E$ ) for graphite of 0.004 (0.4%)	
ENDF/B-VII.0	$0.879 \pm 0.003$
ENDF/B-VI.8	$0.982 \pm 0.003$
JEFF-3.1	$0.912 \pm 0.003$
JENDL-4.0	$0.871 \pm 0.003$
ROI 4 – 1 to 2 MeV with ( $C/E$ ) for graphite of 0.012 (1.2%)	
ENDF/B-VII.0	$0.971 \pm 0.002$
ENDF/B-VI.8	$1.044 \pm 0.002$
JEFF-3.1	$1.003 \pm 0.002$
JENDL-4.0	$0.947 \pm 0.002$
ROI 5 – 0.5 to 1 MeV with ( $C/E$ ) for graphite of 0.037 (3.7%)	
ENDF/B-VII.0	$1.033 \pm 0.002$
ENDF/B-VI.8	$0.993 \pm 0.002$
JEFF-3.1	$1.052 \pm 0.002$
JENDL-4.0	$0.987 \pm 0.002$

The smaller ROI help to highlight the differences in each of the energy regions. Table II reflects that all libraries adequately represent the data in the 10 to 20 MeV ROI, taking into account the large ( $C/E$ ) for graphite in this ROI. ENDF/B-VI.8 provided the best estimate of the neutron interactions between 2 and 10 MeV. The remaining datasets are significantly lower than the measured response. Between 1 and 2 MeV the dataset that best matches the experimental data was JEFF-3.1. ENDF/B-VI.8 overestimates the neutron response where

ENDF/B-VII.0 and JENDL-4.0 underestimate it in this energy region. Between 0.5 and 1 MeV JEFF-3.1 was significantly overestimating the neutron response.

In conclusion, based on the comparisons from Table I and Table II, the library that best agreed with the data for this particular detector at this angle (60 degrees) for  $^{238}\text{U}$  was ENDF/B-VI.8. The new experimental data can be used to further improve  $^{238}\text{U}$  evaluations. Additional data were measured for detectors at scattering angles of 26, 45, 75, 110, 130, and 154 degrees. In general, the same conclusions apply for these additional angles.

## REFERENCES

1. M.B. CHADWICK, et al., “ENDF/B-VII.0: Next Generation Evaluated Nuclear Data Library for Nuclear Science and Technology”, *Nuclear Data Sheets*, **107**, pp. 2931-3060 (2006).
2. A. KONING, et al., The JEFF-3.1 Nuclear Data Library, Nuclear Energy Agency, ISBN 92-64-02314-3 (2006).
3. K. SHIBATA et al., “JENDL-4.0: A New Library for Nuclear Science and Engineering”, *Journal of Nuclear Science and Technology*, **48**, pp. 1–30 (2011).
4. A.B. SMITH and S. CHIBA, “Neutron Scattering from Elemental Uranium and Thorium”, *Ann. Nucl. Energy*, **23**, pp. 459–467 (1996).
5. D.P. BARRY et al., “Quasi-differential Neutron Scattering in Zirconium from 0.5 MeV to 20 MeV”, *Nuclear Science and Engineering*, Submitted For Publication (2011).
6. M.E. OVERBERG, et al., “Photoneutron Target Development for the RPI Linear Accelerator,” *Nuclear Instrumentation & Methods Physics Research A*, **438**, 253 (1999).
7. F.J. SAGLIME III, “High Energy Nuclear Differential Scattering Measurements for Beryllium and Molybdenum”, Ph.D. Thesis, Rensselaer Polytechnic Institute (2009).
8. Scintillator Full Response to Neutron Detection (SCINFUL), PSR-0267, Oak Ridge National Laboratory, (1988).
9. MCNP, A General Monte Carlo Code for Neutron and Photon Transport, Version 5, LA-UR-05-8617 (2005).
10. R. BRUN, F. RADEMAKERS, ROOT an Object Oriented Data Analysis Framework, root.cern.ch/root, (2004).
11. G.F. KNOLL, *Radiation Detection and Measurement*, Wiley & Sons, New York (2000).